Appl. Magn. Reson. 17, 413–431 (1999)

A ^{15}N-^{1}H Dipolar CSA Solid-State NMR Study of Polymorphous Polyglycine (-CO-CD_2-^{15}NH-)$_n$

I. Sack[1], S. Macholl[1], F. Wehrmann[1], J. Albrecht[1], H. H. Limbach[1], F. Fillaux[2], M. H. Baron[2], and G. Buntkowsky[1]

[1] Freie Universität Berlin, Institut für Chemie, Berlin, Germany
[2] LADIR-CNRS, Thiais, France

Received June 4, 1999; revised July 13, 1999

Abstract. The solid-state ^{1}H MAS (magic-angle spinning), ^{2}H static, ^{15}N CP (cross polarization)-MAS and ^{15}N-^{1}H dipolar CSA (chemical shielding anisotropy) NMR (nuclear magnetic resonance) spectra of two different modifications of C_α-deuterated ^{15}N-polyglycine, namely PG I and PG II (-CO-CD_2-^{15}NH-)$_n$ are measured. The data from these spectra are compared to previous NMR, infrared, Raman and inelastic neutron scattering work. The deuteration of C_α eliminates the largest intramolecular ^{1}H-^{1}H dipolar coupling. The effect of the remaining (N)H-(N)H interaction (~5 kHz) is not negligible compared to the ^{15}N-^{1}H coupling (about 10 kHz). Its effect on the dipolar CSA spectra, described as a two-spin system, is analyzed analytically and numerically and it is shown that those parts of the powder spectrum, which correspond to orientations with a strong dipolar ^{15}N-^{1}H interaction, can be described as an effective two-spin system, permitting the measurement of the strength of the ^{15}N-^{1}H dipolar interaction and the orientation of the dipolar vector with respect to the ^{15}N CSA frame. While in the PG II system the ^{15}N CSA tensor is collinear with the amide plane, in the PG I system the CSA tensor is tilted ca. 16° with respect to the ($\delta_{11}\delta_{22}$) CSA plane.

1 Introduction

Poly-α-aminoacids are model systems for the studies of hydrogen bonding in polypeptides and proteins. This is a key factor for the stabilization of secondary and tertiary structures. Polyglycine (-CO-CH_2-NH-)$_n$ is the homopolypeptide of the simplest amino acid. There is no side chain and thus no asymmetric C_α. This polymer is unique for the evaluation of the conformational thermodynamics and the analysis of the spectral features of the backbone [1–4]. In the solid state, polyglycine exhibits structural polymorphism and may adopt two different secondary structures, namely a β-sheet (polyglycine I, PG I) and a 3_1-helix (polyglycine II, PG II) (Fig. 1). These conformations are related to the biologically important structures of collagen, silk fibroin and aperiodic glycine-rich proteins [5–8], as well as nylon materials [9].

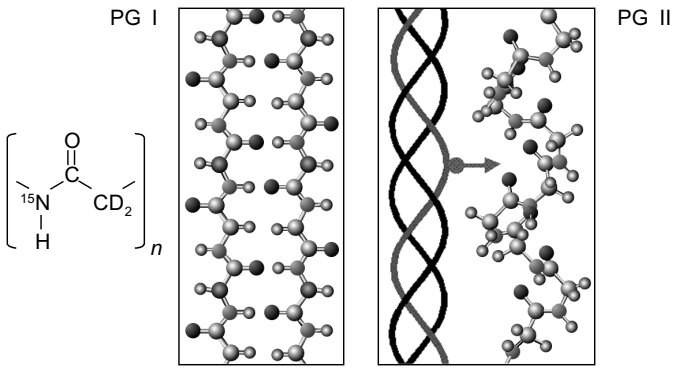

Fig. 1. Chemical structure of polyglycine.

Structural studies of polypeptides are hampered by the disorder inherent to their macromolecular nature. Diffraction studies give only limited information. Polymorphism depending on the molecular weight and sample preparation is an important difficulty for the comparison of data obtained with samples from various origins. Whilst the original proposal of a triple-helical, collagen-like, structure of PG II [10] has never been changed, the structure of PG I has been revised several times. The first structure proposal for the PG I [11] was an anti-parallel β-pleated sheet [12]. Then a modification of the anti-parallel rippled-sheet structure [13] was proposed for a low-molecular-weight polyglycine consisting of about 10 residues [14, 15]. For the high-molecular-weight variety (∼90 residues) [16], longitudinal dislocations of independent crystallites with the same structure were proposed [14]. However, theoretical studies suggest two different three-dimensional structures for the low- and high-molecular-weight PG I [8, 17]. They propose that the low-molecular-weight molecules form a spatial network of hydrogen bonds and have an unusual extended conformation with the mirror-symmetrical residual conformations alternating along the parallel chains and that the high-molecular-weight crystals exhibit a rippled-sheet structure in which chains are antiparallel.

Vibrational spectroscopy techniques are suitable to characterize the relationship between the secondary structure and the hydrogen bond network. They provide information on the dynamics on a very short time scale (10^{-12}–10^{-15} s). Infrared and Raman spectra of amides [18–27] and peptides [1–4, 28, 29] have been thoroughly investigated. The band assignment scheme proposed for the peptide units is based on the amide-like CONH structure [30] engaged in moderately strong hydrogen bonds NH...O with N-O distances of ∼2.8 Å [31]. Totally different structure and dynamics have emerged recently from inelastic neutron scattering (INS) studies of the N-methylacetamide molecule [32, 33], PG I [34, 35] and PG II [36]. The stretching frequency of the hydrogen bond, previously assigned at 3100–3300 cm^{-1}, was reassigned at ∼1550 cm^{-1}, corresponding to a significant increase of the N-H bond length, resulting in an ionic model ($N^{\delta-}...H^{+}...O^{\delta'-}$) instead of the usual covalent representation of the amide hydrogen bond (N-H...O).

For PG II at low temperatures (20 K) a tunneling transition was observed with INS at 40 cm^{-1}. This tunneling transition was interpreted as a tunnel splitting in a symmetric double-well potential along the hydrogen bond [36]. The corresponding potential function has two minima separated by ~0.5 Å and the potential barrier is ~4000 cm^{-1}. The symmetrical double-well potential imposes that protons are not covalently bound to the N or O atoms. The structure of the peptide units should be intermediate between the amide-like and imidol-like models and the mean proton position around the middle of the N...O bond.

Unfortunately, accurate structural data necessary for the characterization of hydrogen bonds in polypeptides cannot be obtained by diffraction techniques and the positions of hydrogen atoms are rather unknown. One way of treating this problem is dipolar solid-state nuclear magnetic resonance (NMR) spectroscopy, resulting in numerous studies of amides, dipeptides, oligopeptides and polypeptides (for example, [37–43]).

The magnetic dipolar interactions between neighboring nuclei depend on both the distances and the orientations of the dipolar vectors with respect to the magnetic field. With single crystals this information can be obtained directly from NMR frequencies measured for different crystal orientations [44, 45]. With non-oriented powder samples, it is still possible to determine distances but the information about the orientation of the dipolar vector is lost, due to the superposition of spectra with different orientations. However, in some cases, the orientation of the dipolar vector can be recovered, employing an internal reference frame (for example the axes of a second NMR interaction tensor or a group of nuclei with known structure). In simple amides the orientations of the ^{15}N chemical shielding anisotropy (CSA) tensor principle axes are directly related to the amide plane. In particular one of the principle axes is the normal to the amide plane, in order to fulfill the constraint of mirror symmetry with respect to the planar amide plane. The NH vector is nearly parallel to the δ_{11} axis of the CSA tensor. For ^{2}H-^{15}N analogues, dipolar couplings in the range of 1600 to 1700 Hz are found, corresponding to typical ND distances between 1.032 and 1.053 Å.

A straightforward analysis of the ^{15}N-^{1}H dipolar CSA NMR powder spectra is possible if the ^{1}H-^{15}N spin pairs can be regarded as isolated. This is the case if the dipolar coupling between the bound ^{1}H-^{15}N is much larger than the homonuclear ^{1}H-^{1}H interaction (in polyglycines ^{15}N-^{15}N dipolar interactions are negligible). For a typical amide proton, the covalent NH bond length R_{NH} is ~1 Å, corresponding to a ^{1}H-^{15}N dipolar coupling constant on the order of d_{NH} ~ 12 kHz.

From the shortest distances between (N)H and (C_α)H of ~2.4 Å, the ^{1}H dipolar coupling constant can be estimated as d_{HH} ~ 9 kHz, which is of the same magnitude as the heteronuclear d_{NH} coupling constant. We therefore removed this coupling by deuteration of the C_α position. In the C_α-deuterated polyglycine, the shortest distances between hydrogen are ~3 Å corresponding to d_{HH} ~ 4 kHz. This coupling is still far from being negligible compared to d_{NH} and gives rise to a multispin system and complex ^{15}N spectra. This is the reason why it is not straightforward to unravel the ^{1}H-^{15}N dipolar coupling and orientation of the ^{1}H-^{15}N vector from the spectra (see below). In principle it is possible to reduce the homonuclear dipolar couplings further by replacing the majority of the amide

protons with deuterons. However, the spectrum of ^{1}H-^{15}N entities would be largely hidden by the signals of the ^{2}H-^{15}N pairs with unknown intensities, due to the cross-polarization (CP) problem. Alternatively it would be possible to apply a homonuclear decoupling of the protons, by applying ^{1}H-^{1}H multipulse decoupling sequences like WAHUHA [46] or MREV8 [47] or Lee-Goldburg decoupling, i.e., radio-frequency (RF) irradiation at the magic angle [48].

The rest of the paper is organized as follows: after a brief summary of the necessary theoretical background of dipolar chemical shift spectroscopy, the experimental details and the sample preparation are presented. Next, the ^{15}N solid state NMR studies of C_α-deuterated and ^{15}N-labeled PG I and PG II (-CO-CD_2-^{15}NH-)$_n$ at room temperature are presented. Employing analytical calculations and numerical simulations it is shown that is possible to extract the size and orientation of the ^{15}N-^{1}H dipolar interaction from these spectra. The orientation of the dipolar vector with respect to the ^{15}N CSA tensor is discussed and finally the most important results are shortly summarized.

2 Dipolar Chemical Shift Spectroscopy

The anisotropic interactions in solid-state NMR can be described by second-rank tensors, i.e., real symmetric 3×3 matrices. For $I = 1/2$ nuclei and nonconducting organic solids the relevant interactions are the chemical shielding tensor $\boldsymbol{\sigma}$, the dipolar interaction tensor $\mathbf{D}$ and the J-coupling (which, however, can in general be neglected in solid-state NMR spectra). For a heteronuclear two-spin system (I, S) the Hamiltonian $\hat{\mathscr{H}}$ for S under the influence of its chemical shielding and of the heteronuclear interaction to I can be written in the usual high-field approximation as [49]:

$$\hat{\mathscr{H}} = \gamma_S B_0 (1 - \sigma_{Szz}) \hat{S}_z + 2 D_{zz} \hat{I}_z \hat{S}_z . \tag{1}$$

All terms in this Hamiltonian commute and it is diagonal with the following eigenvalues:

$$\begin{aligned}
E_1 &= +\frac{1}{2}\gamma_S B_0 (1 - \sigma_{Szz}) + \frac{1}{2} D_{zz}, \\
E_2 &= -\frac{1}{2}\gamma_S B_0 (1 - \sigma_{Szz}) - \frac{1}{2} D_{zz}, \\
E_3 &= +\frac{1}{2}\gamma_S B_0 (1 - \sigma_{Szz}) - \frac{1}{2} D_{zz}, \\
E_4 &= -\frac{1}{2}\gamma_S B_0 (1 - \sigma_{Szz}) + \frac{1}{2} D_{zz}.
\end{aligned} \tag{2}$$

The allowed transitions for spin S are (1-2) and (3-4) with the corresponding transition frequencies:

$$\nu_{\substack{12\\34}}^{S} = \gamma_S B_0(1 - \sigma_{Szz}) \pm D_{zz}. \tag{3}$$

The tensors $\mathbf{D}$ and $\boldsymbol{\sigma}$ can be expressed from their diagonal representation in their principal axis system (PAS) via a rotation $R(\alpha\beta\gamma)$ [50], which can be parameterized using the Euler angles $(\alpha\beta\gamma)$. In general, the CSA and the dipolar interaction tensor have different principal axes and sets of Euler angles:

$$\mathbf{D} = R(\alpha^{\mathrm{D}}\beta^{\mathrm{D}}\gamma^{\mathrm{D}})\mathbf{D}_{\mathrm{PAS}}R(\alpha^{\mathrm{D}}\beta^{\mathrm{D}}\gamma^{\mathrm{D}})^{-1} = R_{\mathrm{D}}\mathbf{D}_{\mathrm{PAS}}R_{\mathrm{D}}^{-1},$$

$$\boldsymbol{\sigma} = R(\alpha^{\mathrm{C}}\beta^{\mathrm{C}}\gamma^{\mathrm{C}})\boldsymbol{\sigma}_{\mathrm{PAS}}R(\alpha^{\mathrm{C}}\beta^{\mathrm{C}}\gamma^{\mathrm{C}})^{-1} = R_{\mathrm{C}}\boldsymbol{\sigma}_{\mathrm{PAS}}R_{\mathrm{C}}^{-1}. \tag{4}$$

It is always possible to transform the dipolar tensor from its principal frame into the frame of the CSA tensor ($\mathbf{D}_{\mathrm{CSA}}$) by a rotation R_{CD} and then to perform a common transformation into the laboratory frame:

$$\mathbf{D} = R_{\mathrm{C}}R_{\mathrm{CD}}\mathbf{D}_{\mathrm{PAS}}R_{\mathrm{CD}}^{-1}R_{\mathrm{C}}^{-1} = R_{\mathrm{C}}\mathbf{D}_{\mathrm{CSA}}R_{\mathrm{C}}^{-1}. \tag{5}$$

Then the dipolar tensor in the CSA frame $\mathbf{D}_{\mathrm{CSA}}$ and the CSA tensor $\boldsymbol{\sigma}$ can be combined to effective shielding tensors $\boldsymbol{\Sigma}_{\mathrm{PAS}}^{\pm}$ in the PAS of $\boldsymbol{\sigma}$, which in general are no longer diagonal:

$$\boldsymbol{\Sigma}_{\mathrm{PAS}}^{\pm} = \boldsymbol{\sigma}_{\mathrm{PAS}} \mp \mathbf{D}_{\mathrm{CSA}} = \boldsymbol{\sigma}_{\mathrm{PAS}} \mp R_{\mathrm{CD}}\mathbf{D}_{\mathrm{PAS}}R_{\mathrm{CD}}^{-1}. \tag{6}$$

After transforming these effective tensors into the laboratory frame, equations for the transition frequencies can be rewritten as:

$$\nu_{\substack{12\\34}}^{S} = \gamma_S B_0(1 - \boldsymbol{\Sigma}_{zz}^{S\pm}). \tag{7}$$

With single crystals, two lines for each spin are observable. For a nonoriented powder sample the average over all orientations has to be calculated. Due to the axial symmetry of the magnetic field, it is sufficient to integrate over two angles $(\vartheta,\ \phi)$:

$$S(\nu) = \int_0^{\pi} \mathrm{d}\,\vartheta \sin\vartheta \int_0^{2\pi} \mathrm{d}\varphi \left(\frac{T_2^S}{1 + 4\pi^2 T_2^{S2}[\nu - \nu_{12}(\vartheta\varphi)]^2} + \frac{T_2^S}{1 + 4\pi^2 T_2^{S2}[\nu - \nu_{34}(\vartheta\varphi)]^2} \right). \tag{8}$$

T_2^S is the transversal relaxation time of the S spins, which for simplicity is assumed to be orientation-independent. Fitting this equation to an experimental dipolar chemical shift spectrum, it is possible to determine the size of the dipolar coupling and the orientation of the dipolar vector with respect to the CSA tensor of spin S.

If the proton is mobile and fast exchange occurs between two proton positions $(a,\ b)$ in a double minimum potential, two limiting cases must be considered.

1. The barrier between the two wells is very high. Then tunneling can be ignored and the measured interaction is the weighted average of the dipolar interaction tensors at each site. If x is the relative population of position a, the average tensor is:

$$\bar{\mathbf{D}} = x\mathbf{D}_a + (1 - x)\mathbf{D}_b. \tag{9}$$

2. In a symmetrical double-well potential with a low barrier, tunneling occurs and the proton is delocalized over the two sites. In the NMR experiment a dipolar interaction averaged over the trajectory of the proton will be measured.

In both cases the strength, the symmetry of the dipolar interaction tensor and the orientation of the averaged dipolar vector are in general different from the dipolar interactions at each position.

3 Experimental

3.1 The Spectrometer

All experiments were performed at a field of 6.98 T, corresponding to a proton resonance frequency of 297.8 MHz on a standard Oxford wide-bore magnet (89 mm) equipped with a room-temperature shim unit. We used a home-built three-channel NMR spectrometer. All three channels are controlled by a pulse programmer with 100 ns resolution, 32-bit binary output and 32 k maximum pulse program length. Each channel consists of a digitally controlled (DDS) synthesizer for generating the NMR frequencies. The necessary phases are generated by directly switching the phase of the digitally controlled synthesizers. After the synthesizer, the actual pulses were generated with fast RF-switches (10 ns rising time) and fed into the power amplifiers. For the proton channel a Creative Electronics 1 kW class C amplifier was used. For the ^{15}N channel a 2 kW class AB amplifier from AMT was employed. All amplifiers are equipped with a RF-blanking for suppressing the noise during data acquisition. All experiments were performed using a commercial 7 mm Bruker triple resonance NMR probe operating at room temperature. To improve the mutual RF isolation of the RF channels commercial band pass filters (Texscan) were employed. The RF of the observed channel was fed through crossed diode duplexer, connected to the detection preamplifier and through the filters into the probe. The other two channels were fed directly through the filters into the probe. Typical 90° pulse width was 7.8 μs for the two channels, corresponding to a B_1-field in frequency units of $\nu_1 = 31.9$ kHz. This was sufficient to remove the ^{1}H-^{15}N dipolar line broadening, due to the reduction of the dipolar coupling by isotope dilution. Repetition time of the experiments was 3 s for the polyglycine. To avoid dead time problems which could cause a distortion of the spectral base line we measured all nonspinning spectra by a fully phase-cycled spin echo technique. The spectra were measured by first cross polarizing the ^{15}N nucleus from the protons and

then recording the spin echo signal under proton decoupling. Typical echo delay was 300 μs. Evaluation of the static NMR powder spectra was performed by expressing the integrals in Eq. (8) for $T_2 = \infty$ in terms of elliptic integrals [44], which are later numerically convoluted with the T_2 decay by Fourier transformation. The referencing of the tensor values against NH_3 was accomplished by determining the isotropic chemical shift value from the ^{15}N CP-MAS (magic-angle spinning) spectra, measured at 5 kHz spinning speed, using the known isotropic shift of PG II (109.1 ppm) [51] as an intermediate reference.

The ^{15}N CP-MAS spectra were recorded at 5 kHz spinning speed. The ^{1}H MAS spectra were recorded at 13 kHz spinning speed with a Bruker 4 mm MAS probe, employing H_2O as an external standard for referencing against TMS. ^{2}H NMR spectra were recorded by applying the quad echo technique with a pulse spacing of 20 μs and a 90° pulse length of 3.5 μs to a home-built 5 mm ^{2}H NMR probe.

3.2 Sample Preparation

Glycine, $H_2{}^{15}NCD_2CO_2H$, was obtained from phthaloyglycine prepared by condensation of potassium ^{15}N-phthalimide (99% ^{15}N purchased from Eurisotop®) and deuterated (>99% D) ethyl bromoacetate. The glycine was purified on Dowex® [52]. The deuteration of the C_α position was controlled with IR, Raman and NMR spectroscopy. The glycine was then polymerized in presence of diphenylphosphorylazide [53], following the procedure of the previous works [34, 36]. PG I was obtained by evaporation of a solution in trifluoroacetic acid. PG II was cast by water from an aqueous solution saturated with LiBr. The secondary structures were controlled with IR spectroscopy. The amounts of disordered domains were less than ~10 and 20% for PG I and PG II, respectively. There is an unknown distribution of molecular weights and in particular the PG I domains can be a mixture of the structures for low and high molecular weights. Bands specific to ends of chains were only barely visible in the IR, suggesting that the averaged chain-length is probably much greater than 10 residues. This result is corroborated by the low spectral intensity in the NH_2 and NH_3^+ region of the CP-MAS spectra (see below).

4 Results

4.1 Experimental Results

4.1.1 MAS Spectra

Figure 2 displays the result of the ^{15}N CP-MAS measurements on PG I and PG II. The full spectra are 20 times enlarged to make small spectral components visible. From these spectra it is evident, that in both systems the main spectral intensity is concentrated in a single line. From these lines the isotropic chemi-

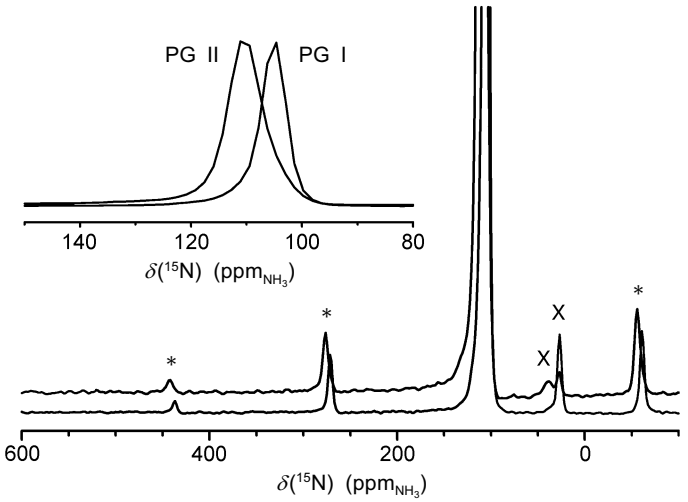

Fig. 2. ^{15}N CP-MAS spectra of PG II and PG I. Shown are the full ^{15}N spectra (intensities 20-fold increased) and an enlargement of the amide region. Estimated isotropic shielding terms are $\delta_{iso}(^{15}N) = 104 \pm 1$ ppm and $\delta_{iso}(^{15}N) = 109 \pm 1$ ppm (inset). The asterisk marks spinning sidebands. The X marks additional spectral intensity, which can be attributed to $-NH_2$ or $-NH_3^+$ groups at the chain ends.

cal shielding values with respect to NH_3 are extracted: $\delta_{iso} = 104 \pm 1$ ppm for PG I and $\delta_{iso} = 109 \pm 1$ ppm for PG II (Fig. 2, inset). The width of the PG II line is approximately twice the width of the PG I line. Except these lines of the amide nitrogen and their rotational side bands some additional spectral intensity is visible in the range of 30 ppm, which can probably be attributed to $-NH_2$ or $-NH_3^+$ groups at the chain ends of the polyglycine strands.

Figure 3 displays the results of the ^1H MAS spectra measured at 13 kHz rotation frequency. The spectral intensity at ca. 1 ppm can be attributed to imperfect deuteration of the C_α. There are clear differences visible between the PG I and PG II samples. Besides the strong line at 4.6 ppm in the PG II sample, whose intensity can be changed by drying on the vacuum line, which we therefore attribute mainly to water, the main spectral intensity is in the range of 6 to 10 ppm and can be attributed to the NH protons. Comparing the PG I and PG II spectra, it is evident that the amide protons are low-field shifted in the PG II sample. Moreover the line of the amide proton seems to be a superposition of different spectral components, which reflect the structural inhomogeneity of the samples.

4.1.2 Static Spectra

The ^2H NMR spectra (not shown) of both modifications were practically identical and displayed a typical -CD spectrum of ca. 125 kHz quadrupolar interaction. Figure 4 displays the experimental (lower line) and simulated (upper line) ^1H-decoupled ^{15}N static powder CP spectra. With the exception of some small

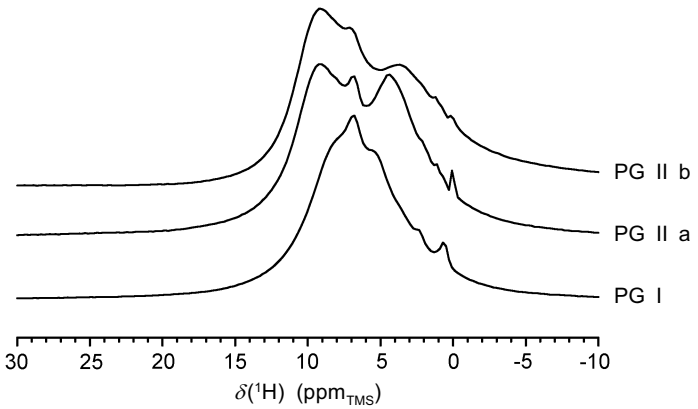

Fig. 3. ^{1}H MAS (13 kHz) spectra of PG I and PG II (a – original sample; b – same sample after drying for one hour on the vacuum line (10^{-6} mbar)).

intensity distortions, which are probably due to different cross polarization efficiencies of the different spectral parts, the simulations give a good reproduction of the experimental data. Some differences in the line shapes are visible. For PG II the CSA tensor is close to axial symmetry. For PG I the shoulder at 60 ppm reveals a deviation from axial symmetry. From the simulations the parameters of the ^{15}N CSA are determined. Figure 5 finally displays the static ^{15}N spectra without ^{1}H decoupling. The spectra exhibit the typical complex behavior

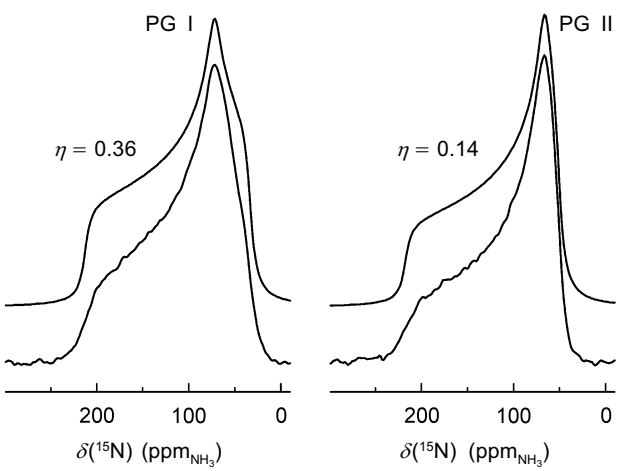

Fig. 4. ^{15}N powder spectra of PG I and PG II under ^{1}H decoupling: experimental (lower line) and simulated (upper line). Parameters for the simulation were: $\delta_{11} = 211 \pm 1$ ppm, $\delta_{22} = 70 \pm 1$ ppm and $\delta_{33} = 31 \pm 1$ ppm for PG I; $\delta_{11} = 216 \pm 1$ ppm, $\delta_{22} = 63 \pm 1$ ppm and $\delta_{33} = 48 \pm 1$ ppm for PG II. The corresponding anisotropy and asymmetry parameters are $\Delta = 160.5$ ppm, $\eta = 0.36$ for PG I, $\Delta = 155.5$ ppm, $\eta = 0.14$ for PG II.

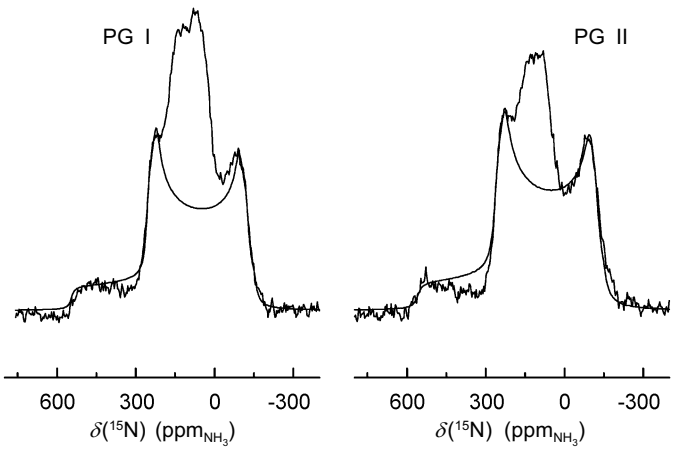

Fig. 5. Superposition of experimental and simulated ^{15}N powder spectra of PG I and PG II without ^{1}H decoupling. The simulation was performed with the CSA parameters from Fig. 4. The strength and orientation of the ^{1}H-^{15}N vector is determined from the outer parts of the spectra. The intensity at the center corresponds to the $\nu_{1,4}$ transitions in Eq. (15) and those crystal orientations where the homonuclear couplings are comparable with the heteronuclear coupling.

of a dipolar chemical shift spectrum, resulting from the superposition of resolved and nonresolved heteronuclear dipolar couplings with the ^{15}N CSA.

4.2 Theoretical Results

As mentioned above, Eq. (1) is the ^{15}N spin Hamiltonian of an isolated ^{1}H-^{15}N spin pair and is only valid if the homonuclear ^{1}H-^{1}H interactions are small, compared to the ^{1}H-^{15}N dipolar interaction. In the following, we want to investigate whether it is allowed to use this approximation in the PG systems also and whether it is possible to extract meaningful information from the ^{1}H-^{15}N dipolar CSA spectra.

The ^{15}N nuclei can be subdivided into two classes, namely those nuclei, where the combined ^{1}H-^{15}N heteronuclear and ^{15}N CSA interaction is stronger than the homonuclear couplings, and the remaining nuclei, which feel more strongly the effect of the other ^{1}H nuclei that are indirectly coupled to the ^{15}N nucleus via the directly bound ^{1}H. The first class consists mainly of those ^{15}N nuclei where the ^{1}H-^{15}N vectors are close to parallel to the external magnetic field. They experience the strongest ^{1}H-^{15}N dipolar interaction and the ^{1}H-^{1}H interaction should be a perturbation to their transition frequency. In the static spectra these nuclei are visible close to the outer singularities of the spectra.

The quantitative features of this model can be studied by investigating a ^{15}N nucleus coupled to two ^{1}H nuclei. The relevant three-spin Hamiltonian is:

$$\hat{\mathscr{H}} = \nu_S \hat{S}_z + 2d_1 \hat{I}_{1z} \hat{S}_z + 2d_2 \hat{I}_{2z} \hat{S}_z + d(2\hat{I}_{1z}\hat{I}_{2z} - \hat{I}_{1x}\hat{I}_{2x} - \hat{I}_{1y}\hat{I}_{2y}) . \qquad (10)$$

$\hat{S}_z$, $\hat{I}_{1k}$ and $\hat{I}_{2k}$, $k = x, y, z$ are the spin operators for ^{15}N and ^{1}H nuclei, respectively. ν_S is the ^{15}N chemical shielding, d the ^{1}H-^{1}H coupling and d_1, d_2 the ^{1}H-^{15}N coupling terms. This Hamiltonian is nondiagonal in the product basis of the single spin wave functions. After transformation into the Liouville representation [49]

$$\hat{\hat{L}} = \hat{\mathscr{H}} \otimes \hat{\hat{E}} - \hat{E} \otimes \hat{\hat{\mathscr{H}}} ,$$

a straightforward calculation reveals that the evolution of the ^{15}N magnetization after either a 90° pulse or a ^{1}H-^{15}N cross polarization (i.e., $\rho(0) = S_x$) occurs in two different three-dimensional subspaces of the Liouville space, which are spanned by the following basis sets:

$$\mathbf{B}1 = \left\{ |\alpha\alpha\alpha\ \beta\alpha\alpha); \frac{|\alpha\alpha\alpha\ \beta\beta\beta) - |\alpha\beta\beta\ \beta\alpha\alpha)}{\sqrt{2}}; |\alpha\beta\beta\ \beta\beta\beta) \right\},$$

$$\mathbf{B}2 = \left\{ |\alpha\alpha\beta\ \beta\alpha\beta); \frac{|\alpha\alpha\beta\ \beta\beta\alpha) - |\alpha\beta\alpha\ \beta\alpha\beta)}{\sqrt{2}}; |\alpha\beta\alpha\ \beta\beta\alpha) \right\}. \tag{11}$$

The Liouville operators in these subspaces are:

$$\hat{\hat{L}}_1 = \begin{pmatrix} \nu + (d_1 + d_2) & -\frac{\sqrt{2}}{4} d & 0 \\ -\frac{\sqrt{2}}{4} d & \nu & \frac{\sqrt{2}}{4} d \\ 0 & \frac{\sqrt{2}}{4} d & \nu - (d_1 + d_2) \end{pmatrix},$$

$$\hat{\hat{L}}_2 = \begin{pmatrix} \nu + (d_1 - d_2) & -\frac{\sqrt{2}}{4} d & 0 \\ -\frac{\sqrt{2}}{4} d & \nu & \frac{\sqrt{2}}{4} d \\ 0 & \frac{\sqrt{2}}{4} d & \nu - (d_1 - d_2) \end{pmatrix}. \tag{12}$$

The signal of the S spin is given as the expectation value of the S_+ operator. Transforming the S_+ operator into these subspaces gives

$$\mathbf{S}1 = [1\ \ 0\ \ 1],$$

$$\mathbf{S}2 = [1\ \ 0\ \ 1]. \tag{13}$$

Diagonalization of the Liouville operators yields the transition frequencies (d_+ and d_- are the sum and difference of the ^{15}N-^{1}H dipolar couplings)

$$\nu_{1,4} = \nu_S,$$

$$\nu_{2,3} = \nu_S \pm \frac{1}{2}\sqrt{d^2 + 4(d_1 + d_2)^2} = \nu_S \pm \frac{1}{2}\sqrt{d^2 + 4d_+^2},$$

$$\nu_{5,6} = \nu_S \pm \frac{1}{2}\sqrt{d^2 + 4(d_1 - d_2)^2} = \nu_S \pm \frac{1}{2}\sqrt{d^2 + 4d_-^2}. \qquad (14)$$

For the class of spins with strong heteronuclear coupling (i.e., $d < d_+$ and $d < d_-$) the square roots in Eq. (14) can be expanded as:

$$\nu_{1,4} = \nu_S,$$

$$\nu_{2,3} \approx \nu_S \pm \left(d_+ + \frac{d^2}{8d_+}\right),$$

$$\nu_{5,6} \approx \nu_S \pm \left(d_- + \frac{d^2}{8d_-}\right). \qquad (15)$$

Therefore, the homonuclear dipolar coupling contributes only in second (quadratic) order to ^{15}N frequencies and can be neglected in first order, in accordance with the concept of "second averaging" [44, 54]. As an example, Fig. 6 shows a calculation of Eq. (14) as a function of the strength of the homonuclear coupling for arbitrary ^{1}H-^{15}N coupling values corresponding to different crystallite orientations with weak, intermediate and strong ^{1}H-^{15}N interaction. The calculations reveal that for strong ^{1}H-^{15}N coupling the effects of the ^{1}H-^{1}H interactions are negligible and the calculated frequencies are practically independent of the homonuclear coupling.

From Eq. (15) it is evident that the homonuclear coupling leads to the presence of spectral intensity at the frequency ν_S of the uncoupled ^{15}N nucleus. The relative line intensities can be calculated as follows.

The two Liouville operators of Eq. (12) can be written as a sum of fictitious spin 1 operators (F_x, F_y, F_z):

$$\hat{\hat{L}}_{\substack{1\\2}} = \nu + \begin{pmatrix} d_\pm & -\frac{\sqrt{2}}{4}d & 0 \\ -\frac{\sqrt{2}}{4}d & 0 & \frac{\sqrt{2}}{4}d \\ 0 & \frac{\sqrt{2}}{4}d & -d_\pm \end{pmatrix} = \nu + d_\pm F_z - \frac{d}{2}(F_z F_x + F_x F_z)$$

$$= \nu + \exp\left(\mathrm{i}\frac{\pi}{2}F_z^2\right)\left(d_\pm F_z - \frac{d}{2}F_y\right)\exp\left(-\mathrm{i}\frac{\pi}{2}F_z^2\right). \qquad (16)$$

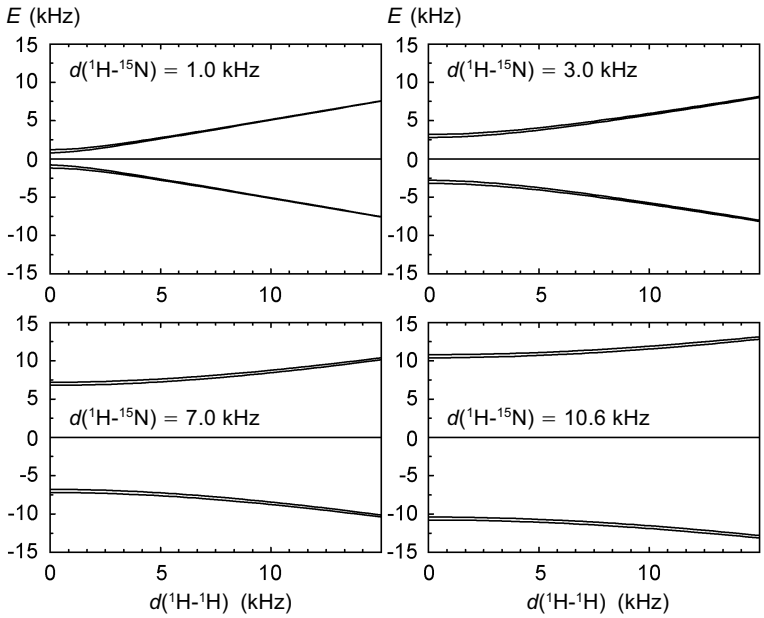

Fig. 6. Calculation of the effect of the dipolar coupling $d(^1\text{H}\text{-}^1\text{H})$ on the ^{15}N frequency, using Eqs. (14) ($\nu_S = 0$ kHz, $d_2 = 0.2$ kHz) for an arbitrary orientation of a crystallite. For the weaker $^1\text{H}\text{-}^{15}\text{N}$ couplings of $d_1 = 1$ and $d_1 = 3$ kHz there is a strong dependence of the ^{15}N frequencies on the $d(^1\text{H}\text{-}^1\text{H})$ coupling. For the strong $^{15}\text{N}\text{-}^1\text{H}$ coupling of $d_1 = 10.6$ kHz frequencies are practically independent of $d(^1\text{H}\text{-}^1\text{H})$, at least below 5 kHz.

Using the abbreviations

$$d_{\text{eff}} = \sqrt{d_{\pm}^2 + \frac{d^2}{4}}, \qquad \cos\varphi = \frac{d_{\pm}}{\sqrt{d_{\pm}^2 + \frac{d^2}{4}}}, \qquad \sin\varphi = \frac{d}{2\sqrt{d_{\pm}^2 + \frac{d^2}{4}}}, \tag{17}$$

Eq. (16) simplifies to:

$$\begin{aligned} L_{\frac{1}{2}} &= \nu + d_{\text{eff}} \exp\left(\mathrm{i}\frac{\pi}{2}F_z^2\right)(F_z\cos\varphi - F_y\sin\varphi)\exp\left(-\mathrm{i}\frac{\pi}{2}F_z^2\right) \\ &= \nu + d_{\text{eff}} \exp\left(\mathrm{i}\frac{\pi}{2}F_z^2\right)\exp(-\mathrm{i}\varphi F_x)F_z\exp(\mathrm{i}\varphi F_x)\exp\left(-\mathrm{i}\frac{\pi}{2}F_z^2\right). \end{aligned} \tag{18}$$

In other words, applying these two transformations diagonalizes the Liouville operators:

$$L_{\frac{1}{2}}^{\text{Diag}} = \nu + d_{\text{eff}}F_z. \tag{19}$$

Transforming Eqs. (13) into this frame gives:

$$S_{\frac{1}{2}}^{\mathrm{Diag}} = \exp(\mathrm{i}\varphi F_x)\exp\left(-\mathrm{i}\frac{\pi}{2}F_z^2\right)S_{\frac{1}{2}}. \tag{20}$$

The intensities of the three transitions finally are given as the square of the intensities of the elements of Eq. (20), which, after some algebra, simplify to:

$$I_{1,4} = 2\sin^2\varphi,$$

$$I_{2,3} = \cos^2\varphi,$$

$$I_{5,6} = \cos^2\varphi. \tag{21}$$

From these transition intensities the powder spectra can be calculated. However in practice it is easier to perform a full numerical simulation of the spectra. Figure 7 shows the result of such a numerical simulation of the effect of the ^{1}H-^{1}H coupling on the ^{15}N spectral line shape of a covalent NH-bond. The spectra were calculated for various homonuclear couplings, varying between 0 and 7 kHz. For the N-H vector an orientation parallel to δ_{33} and for the H-H vector an orientation parallel to δ_{11} was arbitrarily chosen. While the ^{1}H-^{1}H coupling has a strong influence on the central part of the ^{15}N spectrum, the positions of the outer singularities are practically unaffected and can be treated as a two-spin system. Note that the actual form of the central part depends strongly on the relative orientation of the H-H vector with respect to the N-H vector and the ^{15}N CSA frame.

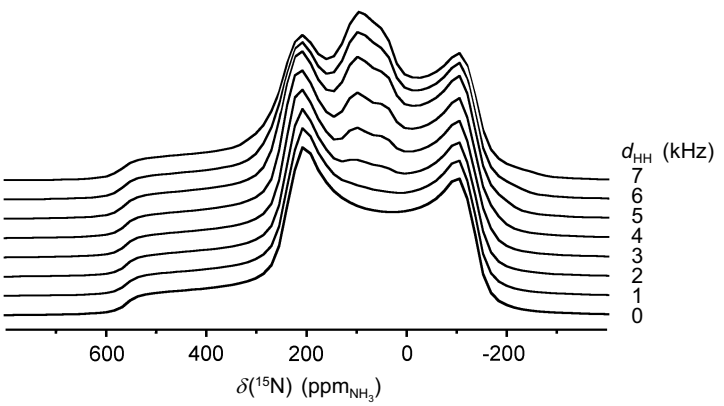

Fig. 7. Numerical simulation of the effect of d_{HH} on a ^{15}N-^{1}H dipolar CSA spectrum using a three spin model (ν_S = 0 kHz, d_2 = 0.2 kHz, d_1 = 10.6 kHz). d_{HH} = 0, 1, 2, 3, 4, 5, 6 and 7 kHz, respectively. For the N-H vector an orientation parallel to d_{33} and for the H-H vector an orientation parallel to δ_{11} was arbitrarily chosen. d_{HH} has a strong influence on the central part of the spectrum, but the positions of the outer singularities are practically unaffected.

5 Discussion

One goal of the NMR study of polyglycine was to find evidence for the proposed hydrogen tunneling process. Therefore the preparation and characterization of the samples used for the NMR experiments were the same as the preparation of samples for the previous INS experiments and similar concentrations of ordered and disordered domains are anticipated. The infrared spectra show that there is a dominant form for each sample, ~80–90% of PG I and PG II, respectively, and domains with ill-defined conformation, supposedly random coil, account for the rest. This structural inhomogeneity is also reflected in the ^{1}H MAS NMR spectra, where, in particular in the PG II sample, several spectral components are visible. In principle by the application of high-speed MAS techniques and combined rotational and multipulse spectroscopy it should be possible to gain enough proton resolution to distinguish between helical structures, β-sheet and random coil regions [55]. The measured isotropic ^{15}N chemical shieldings of the amide nitrogens are typical values for ^{15}N nuclei covalently bound to a proton in an amide, peptide or protein. Their difference of 5 ppm between PG I and PG II corroborates the results of a previous study [51] and can be attributed to the different conformations and hydrogen bonding situations. However there are differences in the anisotropy and asymmetry of the measured tensors compared to the previous study: $\Delta = 160.5$ ppm, $\eta = 0.36$ for PG I and $\Delta = 155.5$ ppm, $\eta = 0.14$ for PG II instead of $\Delta = 152$ ppm, $\eta = 0.15$ for PG I and $\Delta = 158$ ppm, $\eta = 0.12$ for PG II [51].

Singularities at ca. 600 ppm reveal covalent NH-bonds with a rather large ^{1}H-^{15}N coupling. Employing the ^{15}N CSA data from the ^{1}H decoupled spectra, Eq. (8) is employed to determine the size and orientation of the ^{15}N-^{1}H vector in the CSA frame. The major dipolar coupling values are very similar for both modifications: $D = 10.4 \pm 0.3$ kHz for PG I and $D = 10.6 \pm 0.3$ kHz for PG II. They correspond to similar covalent bonds with distances $R_{NH} = 1.054$ and 1.047 ± 0.01 Å, respectively. However, the orientation of the N-H vector with respect to the PAS of the ^{15}N CSA tensor is different for the two modifications (Fig. 8). For PG II the ^{15}N-^{1}H vector is in the (δ_{11}, δ_{22}) plane ($\beta = 90 \pm 2°$, $\alpha = 19 \pm 3°$). For PG I ($\beta = 74 \pm 2°$, $\alpha = 12 \pm 2°$), the ^{15}N-^{1}H vector is rotated by 16° out of the (δ_{11}, δ_{22}) plane.

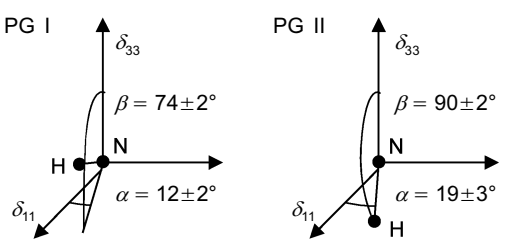

Fig. 8. Sketch of the orientation of the ^{1}H-^{15}N dipolar vector in the ^{15}N CSA frame. PG I: $D = 10.4 \pm 0.2$ kHz, $R_{NH} = 1.054 \pm 0.007$ Å. PG II: $D = 10.6 \pm 0.2$ kHz, $R_{NH} = 1.047 \pm 0.007$ Å.

The profiles calculated in the two-spin approximation account only for the outer parts of the spectra. The intensity distortion between 300 and 400 ppm may again be due to different cross polarization efficiencies.

In the central part of the undecoupled spectra there are strong deviations between experimental and simulated spectra. In principle, there are two different reasons for this additional intensity, which are not necessarily mutually exclusive.

1. The intensity stems from ^{15}N nuclei which experience only a weak dipolar coupling, either because the distance to the amide proton is increased for these nuclei or because a mobile amide proton is exchanging fast between positions with different dipolar coupling. In the latter case a weakened average dipolar coupling would be measured, resulting in a more narrow line width [54].

2. The homonuclear dipolar interactions among the protons lead to a fast spin exchange of the protons, which effectively decouples these ^{15}N nuclei from the protons [56].

From the static spectra alone it is not possible to decide between these two alternatives. Because the isotropic chemical shielding of an unprotonated ^{15}N nucleus exhibits a low-field shift, compared to a protonated nitrogen, the ^{15}N CP-MAS spectra can help to decide between these two alternatives. The absence of spectral intensity in the ^{15}N CP-MAS spectra lowfield of the line of the covalently bound amide nitrogen suggests the second alternative as the more probable one.

For PG II the orientation of the dipolar vector in the CSA frame is similar to that reported for the N-octyl-D-gluconamide molecule ($\alpha = 15°$, $\beta = 90°$) [42]. δ_{33} is perpendicular to the amide plane containing δ_{22} and δ_{11}. The direction of the amide bond in the (δ_{11}, δ_{22}) plane is determined by the angle α between the NH bond and the δ_{11}-axis (Fig. 8). For PG I the ^{15}N-^{1}H vector is not in the (δ_{11}, δ_{22}) plane ($\alpha = 12°$, $\beta = 74°$). The β angle determines the tilt of the CSA tensor with respect to the amide plane (for $\beta = 0$ or $\beta = 90°$ two of the principle axes lie in the amide plane, $\beta = 74°$, the tensor is tilted 16° with respect of the amide plane). There exist several possible reasons for this tilt.

1. The CSA tensor is in the CO-N-C_α plane of the peptide group, but the hydrogen is rotated out of this plane, leading to a nonplanar structure of the peptide group. This structure can occur either due to a fast proton exchange or because of a static displacement of the proton in the hydrogen bond.

2. The hydrogen is in the CO-N-C_α plane, i.e., the peptide group is planar, but the CSA tensor is rotated out of the plane or both CSA tensor and hydrogen atom are rotated out of the CO-N-C_α plane.

In the fast exchange regime the dipolar coupling should be averaged. Owing to the axial symmetry of the dipolar interaction, a rotation around an axis perpendicular to the dipolar vector is necessary to change the orientation of the effective tensor. The maximum averaged dipolar coupling can be estimated from Eq. (9) (assuming a symmetric exchange):

$$\overline{D} = \frac{D}{4}(1 + 3\cos\varphi) \tag{22}$$

and

$$\overline{R}^{-3} = \frac{R_{\mathrm{NH}}^{-3}}{4}(1 + 3\cos\varphi) \,. \tag{23}$$

With $\varphi = 2\beta = 32°$ and $\overline{D}$ = 10.4 kHz, then D = 11.7 kHz and R_{NH} = 1.015 Å. This NH bond length is too short to be reasonable. Thus a dynamic exchange of the proton can be excluded as the main reason of the tilt of the CSA vector.

If a static displacement of the amide of the amide proton has occurred, for example due to the proposed exchange between amide- (a) and imidol-like (b) forms, an approximately linear change of the NH distance takes place, leading to an averaging of the dipolar interactions:

$$\overline{D} = \frac{1}{2}(D_{\mathrm{a}} + D_{\mathrm{b}}) \,,$$

$$\overline{R}^{-3} = \frac{1}{2}(R_{\mathrm{NHa}}^{-3} + R_{\mathrm{NHb}}^{-3}) \,. \tag{24}$$

Using $R_{\mathrm{NHa}} \sim 1$ Å and $R_{\mathrm{NHb}} \sim 1.5$ Å, an average distance of $\overline{R} \sim 1.16$ Å corresponding to an average dipolar coupling of $\overline{D} \sim 8$ kHz is estimated. This latter value is quite different from the observed $\overline{D} \sim 10$ kHz. Thus one can exclude a symmetric fast exchange for these protons and a lower bound for the probability of the amide-like structure can be estimated as 90%.

The second explanation finally is that the CSA tensor is tilted with respect to the amide plane. In a recent study the orientation of the CSA tensors of various di- and tripeptides and collagen is summarized [57]. For several of these tensors a tilt with respect to the amide plane is observed, showing that in these systems the CSA tensor is not necessarily coplanar with the amide plane. The reported tilt angles range from 17.6 to 25.5°. Comparing this to our result of $\beta = 74 \pm 2°$, i.e., a tilt angle of 16° we conclude that a similar rotation of the CSA tensor has also occurred in our system, i.e., the position of the amide hydrogen has not changed and the ^{15}N CSA tensor is not coplanar with the amide plane.

6 Conclusion

C_α-deuteration of ^{15}N-polyglycines (-CO-CD_2-^{15}NH-)$_n$ eliminates the main H-H homonuclear dipolar interactions between (C_α)H and (N)H but the remaining homonuclear interactions between (N)H atoms, compared to the H-^{15}N coupling, remain large enough to perturb the ^{15}N NMR spectra. Nevertheless the data can be partially analyzed as effective two-spin systems. The best fits to the observed spectra give ^{1}H-^{15}N dipolar coupling of $\sim$10 kHz corresponding to protons covalently bound to nitrogen atoms with $R \sim 1.05$ Å. There is no evidence for fast dynamical exchange between two proton sites. While in the PG II system the

^{15}N CSA tensor is collinear with the amide plane, in the PG I system the CSA tensor is tilted with respect to the CSA plane.

Acknowledgements

This work was supported by the Deutsche Forschungsgemeinschaft Grant: Sonderforschungsbereich 448 “Mesoskopisch Strukturierte Verbundsysteme” and the German-Israel Foundation Grant GIF I-595-43.09/98. Here we should like to thank M. F. Lautié from LADIR-CNRS for the sample preparation.

References

1. Krimm S., Abe Y.: Proc. Natl. Acad. Sci. USA **304**, 170 (1972)
2. Fanconi B., Finegold L.: Science **190**, 458 (1975)
3. Finegold L., Kumar P.K.: Biopolymers **19**, 1567 (1980)
4. Gresh N., Giessner-Prettre C.: Biochem. Biophys. Res. Commun. **171**, 1211 (1990)
5. Gomes J., Sanchez-Martinez D., Stiefel V., Rigau J., Puigdomenec P., Pages M.: Nature **334**, 262 (1988)
6. Cretin C., Puigdomenec P.: Plant Mol. Biol. **15**, 783 (1990)
7. Lei M., Wu R.: Plant Mol. Biol. **16**, 187 (1991)
8. Kajava A.V.: Acta Crystallogr. Sect. D **54** (1998)
9. Tormo J., Puigali J., Vives J., Fita I., Lloveras J., Bella J., Aymani J., Subirana J.A.: Biopolymers **32**, 643 (1992)
10. Crick F.H.C., Rich A.: Nature **176**, 780 (1955)
11. Astbury W.T.: Nature **163**, 722 (1949)
12. Pauling L., Corey R.B.: Proc. R. Soc. London, Ser. B **141**, 21 (1953)
13. Pauling L., Corey R.B.: Proc. Natl. Acad. Sci. USA **39**, 253 (1953)
14. Lotz B.J.: J. Mol. Biol. **87**, 169–180 (1974)
15. Collonna-Cesari F., Premillat S., Lotz B.: J. Mol. Biol. **87**, 181 (1974)
16. Munoz-Guerra S., Puiggali J., Rodrigues A., Suburana J.A.: J. Mol. Biol. **167**, 223 (1983)
17. Kajava A.V.: Biofizika **30**, 406 (1985)
18. Miyazawa T., Shimanoushi S., Mizushima S.: J. Chem. Phys. **29**, 611 (1958)
19. Pivcova H., Schneider B., Stok J.: Coll. Czech. Chem. Commun. **30**, 2215 (1965)
20. Schneider B., Horeni A., Pivcova H., Honzl J.: Coll. Czech. Chem. Commun. **30**, 2196 (1965)
21. Itoh K., Shimanoushi T.: Biopolymers **5**, 921 (1967)
22. Miyazawa T.: Poly-α-aminoacids (Fasman Dekker G., ed.), p. 69. New York: Dekker 1967.
23. Jakes J., Krimm S.: Spectrochim. Acta A **27**, 19 (1971)
24. Rey-Lafon M., Forel M.T., Garrigou-Lagrange C.: Spectrochim. Acta A **29**, 471 (1973)
25. Cheam T.C., Krimm S.: J. Chem. Phys. **82**, 1631 (1985)
26. Fillaux F., Baron M.H., de Loz C., Sagon G.: J. Raman Spectrosc. **7**, 244 (1978)
27. Fillaux F., Baron M.H.: Chem. Phys. **62**, 275 (1981)
28. Krimm S.: Nature **212**, 1482 (1967)
29. Krimm S., Bandekar J.: Adv. Protein Chem. **38**, 181 (1986)
30. Pauling L.: The Nature of the Chemical Bond, p. 281. Ithaca, NY: Cornell Univ. Press 1960.
31. Katz J.L., Post B.: Acta Crystallogr. **13**, 624 (1960)
32. Fillaux F., Fontaine J.P., Baron M.H., Kearley G.J., Tomkinson J.: Chem. Phys. **176**, 249 (1993)
33. Fillaux F., Baron M.H., Nicola B., Tomkinson J., Kearley G.J. in: Biological Macromolecular Dynamics (Cusack S., Büttner H., Ferrand M., Langan P., Timmins P., eds.), p. 69. Schenectady, NY: Adenine Press 1997.
34. Fillaux F., Fontaine J.P., Baron M.H., Leygue N., Kearley G.J., Tomkinson J.: Biophys. Chem. **53**, 155–168 (1994)

35. Kearley G.J., Fillaux F., Baron M.H., Bennington S., Tomkinson J.: Science **264**, 1285–1289 (1994)
36. Fillaux F., Nicolai B., Baron M.H., Lautie A., Tomkinson J., Kearly G.J.: Ber. Bunsenges. Phys. Chem. **102**, 384–392 (1998)
37. Ando S., Ando I., Shoji A., Ozaki T., Tabeta R., Saito H.J.: J. Am. Chem. Soc. **107**, 7848 (1985)
38. Ando S., Yamanobe T., Ando I., Shoji A., Ozaki T.: J. Mol. Struct. **192**, 153 (1989)
39. Shoji A., Ozaki T., Fujito T., Deguchi K., Ando S., Ando I.: Macromolecules **22**, 2860 (1989)
40. Asakawa N., Kuroki S., Kurosu H., Ando I., Shoji A., Ozaki T.: J. Am. Chem. Soc. **114**, 3261 (1992)
41. Lumsden M.D., Wasylishen R.E., Eichele K., Schindler M., Penner G.H., Power W.P., Curtis R.D.: J. Am. Chem. Soc. **116**, 1403 (1994)
42. Buntkowsky G., Sack I., Limbach H.-H., Kling B., Fuhrhop J.: J. Phys. Chem. B **101**, 11265 (1997)
43. Sitkoff D., Case D.A.: Prog. NMR Spectrosc. **32**, 165 (1998)
44. Haeberlen U.: High Resolution NMR in Solids: Selective Averaging. Advances in Magnetic Resonance Supplement 1. New York: Academic Press 1976.
45. Mehring M.: High Resolution NMR Spectroscopy in Solids. Berlin: Springer 1983.
46. Waugh J.S., Huber L.M., Haeberlen U.: Phys. Rev. Lett. **20**, 180 (1968)
47. Rhim W.-K., Elleman E., Vaughan R.W.: J. Chem. Phys. **59**, 3740 (1973)
48. Lee M., Goldburg W.I.: Phys. Rev. A **140**, 1261 (1965)
49. Ernst R., Bodenhausen G., Wokaun A.: Principles of NMR in One and Two Dimensions. Oxford: Clarendon Press 1987.
50. Rose M.E.: Elementary Theory of Angular Momentum. New York: Wiley 1957.
51. Shoji A., Ando A., Kuroki S., Ando I., Webb G.: Annu. Rep. NMR Spectrosc. **26**, 58 (1993)
52. Armarego W.L.F., Milloy B.A., Pendergast W.: J. Chem. Soc. Perkin I, 2229 (1976)
53. Nishi N., Tsunemi M.: Makromol. Chem. **192**, 1789 (1991)
54. Schmidt-Rohr K., Spiess H.W.: Multidimensional Solid State NMR and Polymers. London: Academic Press 1994.
55. Lee D.K., Ramamoorthy A.: J. Phys. Chem. B **103**, 271 (1999)
56. Slichter C.P.: Principles of Magnetic Resonance, 3rd edn. Berlin: Springer 1990.
57. Lee D.K., Wittebort R.J., Ramamoorthy A.: J. Am. Chem. Soc. **120**, 8868 (1998)

Authors' address: Gerd Buntkowsky, Institut für Chemie, Freie Universität Berlin, Takustrasse 3, D-14195 Berlin, Germany